Development of a Method for Measuring Charged Particle Beam Fluence Beyond 10^{16} 1-MeV-neutron equivalent/cm^2

By

Nelly Aylon

Undergraduate Honors Thesis

Mentors: Sally Seidel and Martin Hoeferkamp

Physics and Astronomy Department
University of New Mexico

April 22, 2016

Abstract

A device has been prototyped for measuring remotely and in real time the profile of a charged particle beam and the fluence it delivers to a target. The device was prototyped by building and operating an array of “3D” silicon diodes. 3D silicon sensors are p-n junction-based electronic devices with high tolerance to radiation and durability over time. The motivation for this research is preparation for experiments at the Large Hadron Collider at CERN, an instrument for studying and discovering new particles and forces. This collider will be upgraded in 2024. The upgrade will increase the rate of particle collisions by a factor of 10. Elements of detectors at the collider must be tested in advance to assess their responses to radiation at fluences up to $1x10^{16}$ 1-MeV-n-eq/cm^2. To simulate the damage from particles produced in the collider, the 3D diode array was exposed to a proton beam at Los Alamos National Laboratory. The fluence applied to the sensors was determined by analyzing the leakage current of each sensor as a function of beam exposure time. The potential for imaging the beam profile and measuring its fluence in real time was demonstrated.

Contents

I. Introduction

A device was developed for measuring remotely and in real time the profile of a charged particle beam and the fluence it delivers to a target. The device was prototyped by building and operating an array of “3D” silicon diodes. The device was tested with an 800 MeV proton beam at the Los Alamos Neutron Science Center (LANSCE). The fluence applied to the sensors was determined by analyzing the leakage current of each sensor as a function of beam exposure time. The potential for imaging the beam profile and measuring its fluence in real time was demonstrated.

1.1 The Large Hadron Collider

The Large Hadron Collider (LHC) is part of the European Organization for Nuclear Research (CERN) accelerator complex. It is currently the world’s largest and most powerful particle accelerator. The LHC is used by a worldwide community of over 10000 engineers and scientists from more than 100 countries. The LHC is a 27 km ring of superconducting magnets located 145 m under the French-Swiss Border. There are several structures that serve to accelerate the beam. The devices increase the beam’s particle energy before the collision.

The accelerator sends 2 particle beams through different beam pipes. Figure 1 shows the beam pipe at the LHC.The beams are accelerated until they are close to the speed of light. The superconducting magnets guide the beams through the beam pipe. Finally just before the collision quadrupole magnets are used to focus the particles and increase the collision probability.

The beams collide at 4 points on the 27 km circumference. The major experiments at the LHC are located at the beam collision areas. The experiments are: ATLAS, CMS, ALICE, and LHCb.

Figure 1- Beam pipe at the LHC 145m under the earth’s surface

1.2 ATLAS

A Toroidal LHC Apparatus or ATLAS is a general purpose detector located at the LHC. The detector was built and is used by a worldwide collaboration involving 3000 people, 174 institutions and 38 countries. The ATLAS experiment seeks answers to fundamental questions about matter, forces and symmetry. The Standard Model is a theory that describes the world. It is a simple and comprehensive theory that explains all the hundreds of particles and complex interactions with only: 6 quarks, 6 leptons, force-transmitters, and the Higgs boson that produces mass. The scientists at ATLAS test the Standard Model predictions and search for new physics processes.
The ATLAS detector has dimensions: 46m long, 25m high, and 25m wide. It weighs over 7000 tonnes. The particle beams collide at the center of the ATLAS detector. New particles, products of the collisions, travel in every direction. To detect the particles and record their characteristics, the ATLAS detector has 3 main detector systems:

- Inner Detector: For high accuracy measurements of particle trajectories
- Calorimeter: Measures the energies of charged and neutral particles
- Muon spectrometer: Measures muon paths to determine their momentum

Figure 2 shows the ATLAS detector schematically with its main detector systems. The Inner Detector is as close to the beam collisions as 55 mm. The Muon Chambers are 11m away from the collisions[1].

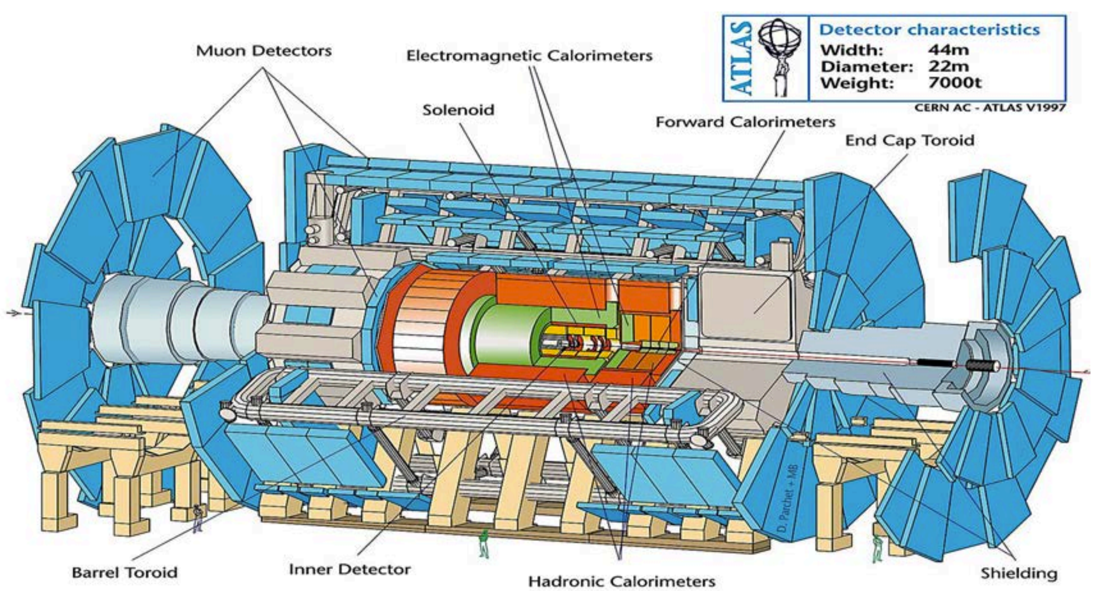

Figure 2-The ATLAS detector, schematic view, showing its main detector systems.

1.3 High Luminosity Large Hadron Collider

The LHC has been running since 2010, and has produced several scientific discoveries in High Energy Physics (HEP). The LHC started producing proton collisions of 7-8 TeV in 2010. As shown in Figure 3, the LHC schedule includes several upgrades to improve its performance. The LHC will be upgraded to the High Luminosity-LHC (HL-LHC) in 2020.The HL-LHC will increase the collision rate by a factor of 10, allowing researchers to observe rarer events. The collision rate will increase from 10^{34} $cm^{-2}s^{-1}$ to 10^{35} $cm^{-2}s^{-1}$. The uncertainties will also be reduced due to the higher statistics of the measurements.
The upgrade to the HL-LHC presents a challenge. The challenge will not only come from the modifications to the LHC, but also the related upgrade to the ATLAS detector components. The increase in luminosity will produce a significant increase in fluence to the devices installed in the ATLAS detector. The increase in fluence will damage the devices. This damage will decrease the amount of signal detected and increase the noise. The devices require improved radiation hardness characteristics to be able to operate successfully during the remainder at the LHC lifetime.

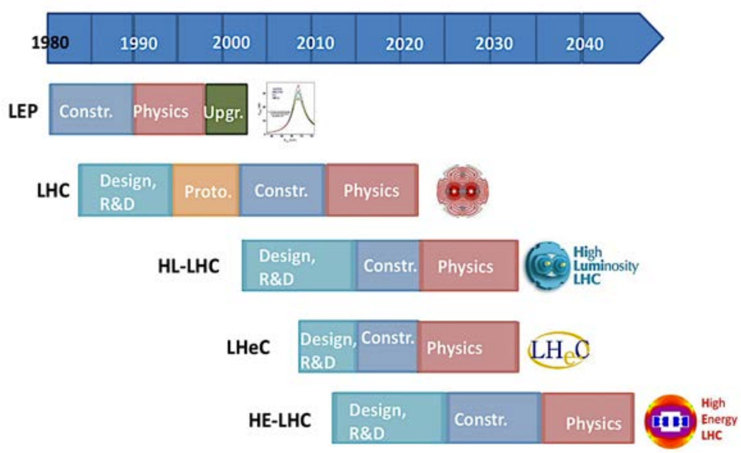

Figure 3- LHC timeline

1.4 Motivation for the study

Experimental devices that are going to be exposed to high doses of radiation, such as at the Large Hadron Collider, must be radiation hard. All the devices must be tested in advance to assess their responses to radiation. Particle beams can be used to irradiate devices to high fluences. Imaging the beam profile and measuring its fluence in real time can be a challenge, especially for fluences greater than 10^{16} 1-MeV-neutron equivalent/cm^2 [2].

3D silicon sensors are electronic devices with high tolerance to radiation. Previous studies [3,4] that investigated 3D sensors demonstrated their leakage current's linear response to radiation according to Eq (1):

$$\Delta I = \alpha \, \Phi_{eq} \, V \qquad (1)$$

In Eq (1) ΔI is the change in leakage current, α is a factor that depends in time and temperature, V is the volume of the device, and Φ_{eq} is the fluence normalized to that of 1-MeV-neutrons in damage potential.

The temperature has a significant effect upon the leakage current recorded for a silicon detector. Eq (2) shows the formula for a scale factor

$$\theta(T_a) = \exp\left(-\frac{E_g}{k_B}\left(\frac{1}{T_a} - \frac{1}{T_{ref}}\right)\right) \quad (2).$$

If the current is recorded at temperature T_a, it must be scaled to its respective value for temperature T_{ref} by multiplying by $\theta(T_a)$. The factor E_g=1.23 eV is the silicon band gap energy and k_B is the Boltzmann constant.

When the two charged particle beams at the LHC collide, free quarks dominantly form pions in the final state. These pions are the main source of radiation that damages the devices in the detectors. Proton and pion damage are nearely identical for track energies beyond 10^2 MeV. The typical track energy in the LHC. For that reason it is possible to use a proton beam to simulate pion damage. An 800 MeV proton beam was used to test the device constructed with 3D silicon sensors.

The measurements of fluence are given in 1-MeV-neutron equivalent. The damage produced by a hadron is a complicated process that involves the dislocation of atoms from their lattice sites, atomic recoil, ionization, heating, production of complex crystallographic defects, and other things. The conversion between neutrons and proton in terms of their ability to damage the material is characterized by the hardness factor which is 0.71 for 800 MeV protons.

II. 3D Silicon sensors

2.1 Description

3D silicon sensors are p-n junction-based electronic devices with high tolerance to radiation and durability over time. The p-type and n-type junctions are micro-machined into the intrinsic Si substrate in columns perpendicular to the substrate surface. The wafer has a resistivity that ranges from 10 to 30 kΩ-cm. To operate, the sensors must have a bias potential applied between their n- and p-type electrodes. The breakdown voltage (V_{bd}) is found with a measurement of current versus bias voltage (IV). The depletion voltage (V_d) is found with a measurement of bulk capacitance versus bias voltage (CV). The operating voltage is between V_d and V_{bd}. 3D detectors require low bias voltage to be operated. The sensors used were fabricated by FBK (Trento, Italy).

Radiation causes defects in the silicon crystal of the sensors. These defects trap the charge signal that should be collected. By raising the bias voltage the charge can be liberated from the traps. At a certain point, increasing the bias voltage to higher values will produce electrical breakdown of the detectors.

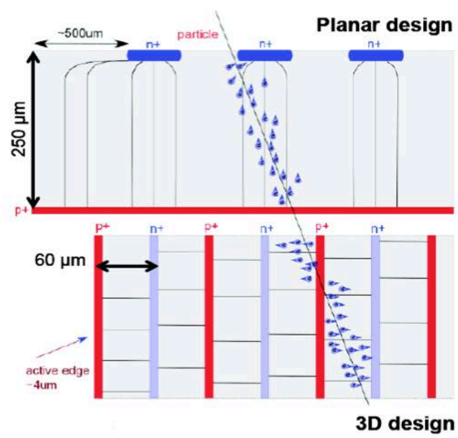

Figure 4- Planar and 3D cross section diagram

2.2 3D versus Planar

Planar silicon sensors are the geometry typically used before the 3D design was invented. Fig. 4 shows the physical difference between the 3D and planar design. The planar design has n-type and p-type strips on the top and bottom surface of the silicon sensor parallel to the wafer's surface. The 3D design has n-type and p-type columns throughout the silicon wafer's thickness. The thickness of the wafers in either of the sensors is in the range 230-250μm.
The planar design is a more mature technology that has a higher yield and a lower cost. Micromachining the columns in the 3D design is a manufacturing challenge. The 3D design typically has a yield above 60%[4].
The distance between the electrodes in the planar design is close to 250μm, the thickness of the silicon. The 3D design has a distance between electrodes of 60μm. The main benefit of the 3D design is the short distance between the electrodes. The short distance between electrodes allows the sensor to deplete at a lower voltage, allows free charges to be collected faster, and reduces the amount of free charge trapped in the silicon crystal's defects.

The 3D design advantage of lower V_d has significant benefits due to the importance of operating the silicon sensors above depletion but below breakdown. The V_d of a sensor will increase when it is exposed to radiation. The bias voltage applied to the sensor for proper operation will have to increase as a function of radiation exposure, but at the same time the leakage current flowing though the sensor at a certain voltage will be higher after irradiation. The high leakage current may at some point produce electrical breakdown in the sensor. After this point the sensor would not be able to collect any data.

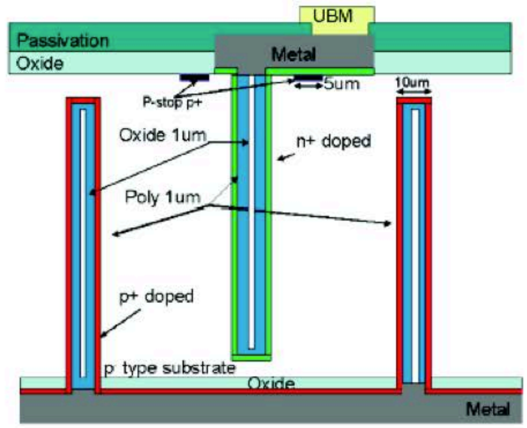

Figure 5- 3D sensors used in the experiment

The 3D sensors used for this experiment have a cross section like the one shown in Fig 5. The electrode columns are etched from both sides; they do not go all the way through. The wafer thickness was measured to be $190 \pm 61 \mu m$. The production yield of this design is higher than the yield of a 3D sensor in which the columns pass all the way through the substrate. This design has a V_d lower than 15V before irradiation and 180V at the end of life.

2.3 IV and CV measurements

The leakage current versus bias voltage (IV) and capacitance versus bias voltage (CV) measurements determine V_d and V_{bd} respectively. The CV measurements were performed by mounting the sensors onto a chuck in a probe station and applying increasing bias voltage while recording the capacitance. Figure 6 shows an example of a CV measurement on two of the sensors used for the experiment. The V_d is extracted from the inverted plateau of the graph. V_d is also the minimum bias voltage required for the sensor's normal operation.
The IV measurements were performed on the sensors by increasing the bias voltage while recording the leakage current. The V_{bd} is defined as the point at which the leakage current is 3 times greater than the leakage current of depletion. V_{bd} is often the bias voltage at which the leakage current increases exponentially, and it is the absolute maximum bias voltage which can be applied to the sensor for normal operation. The IV measurements of the devices used in the experiment are plotted in Figure 7.

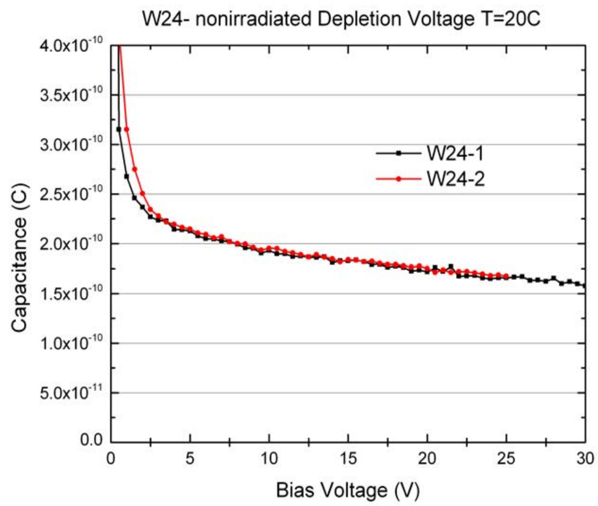

Figure 6- CV measurement of sensor 2 from wafer 24 (W24-2) and sensor 1 from wafer 24 (W24-1)

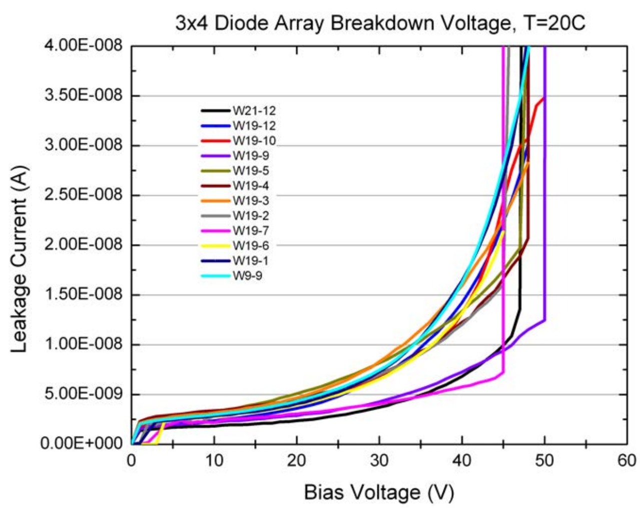

Figure 7- IV measurements of each 3D sensor used in the experiment

III. Experiment

The first step of the experiment was to receive the 3D diodes and evaluate their characteristics. Twenty sensors were evaluated in this analysis. IV and CV measurements were performed to determine depletion and breakdown. The 12 sensors with the largest operating window were selected. Appendix 1 displays the IV and CV measurements for all the diodes.

According to Eq.1 the volume of the diode is a necessary quantity to calculate the fluence. The x and y dimensions were measured using a microscope and software that displayed the sensor on a computer screen. Figure 8 shows a picture of the top part of the sensor.

The microscope optics allow the operator to measure the thickness of the sensors. The microscope was first focused on the flat surface where the sensor rests. The height of the microscope was set to 0. The microscope was slowly retracted until it was focused in the top of the sensor. The value of the z dimension is equal to the z position of the microscope.

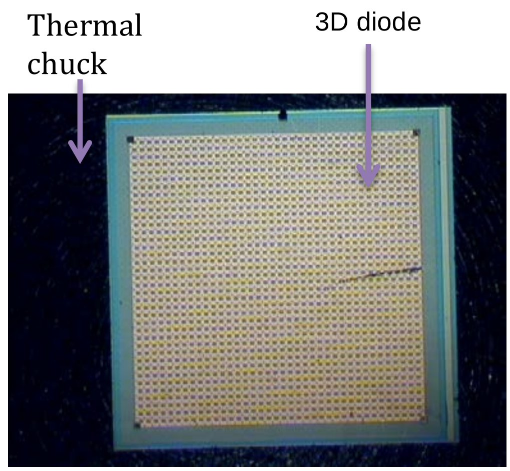

Figure 8- Top side of a 3D diode

3.1 Setup

The twelve 3D sensors were arranged in a 3x4 array in a printed circuit (PC) board with metallization to mount and read out the diodes (see Figure 11). The PC board contacts were plated with gold to allow wirebonding. The sensors were wire bonded to the printed circuit board from the top part; the bottom part of the sensor was attached with conductive epoxy.

Two wire bonds were made for each sensor, each from a different sensor pad. Figure 9 shows one of the 3D sensors of the array attached to the PC board with the conductive epoxy underneath and the wire bonds above.

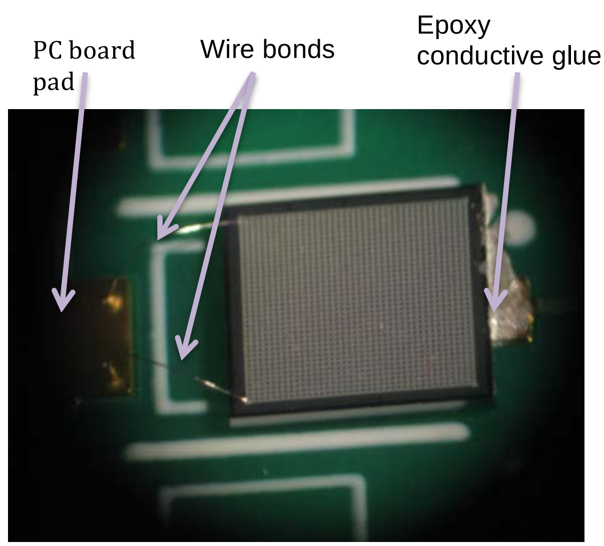

Figure 9-3D sensor attached to the PC board

The setup to operate the diode array is shown in Figure 10. The PC board was connected by a 30m long ribbon cable to the Keithley 6487 voltage source/current measure unit. The Keithley 706 scanner is interfaced with a Keithley 7158 low current scanner, controlled with LabVIEW software. The program allowed the operator to measure the leakage current of the 12 diodes one by one by closing/opening each channel in the Keithley 7158 low current switches.

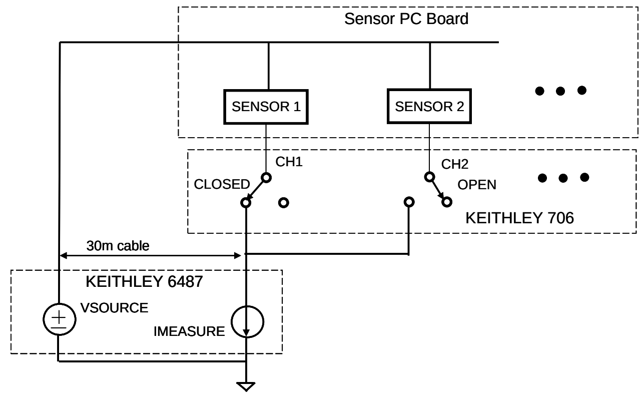

Figure 10- Setup for operating the diode array

The 30m long ribbon cable interfaced to 12 BNC coaxial cables using a special interface box, and each coaxial cable carried the current of one sensor element of the 3x4 array. Each sensor was connected to an input channel of the Keithley 706 through the Keithley 7158 low current switches. The 3D sensors had currents in the range 10^{-7}-10^{-9} A before and after irradiation. Each channel could be opened (disabling the connection) or closed (enabling the connection).

Finally the Keithley 6487 was connected to the PC board with the appropiate bias voltage. The Keithley 6487 was also connected to the switched output displaying the leakage current readout. The setup was completed and tested before the experiment in LANSCE.

After the setup was built, the diode array was exposed to a proton beam. The diode array was placed facing the proton beam at LANSCE. The total exposure to the proton beam was received in several exposure intervals or runs. In between the runs the leakage current of each sensor at the appropriate operating voltage was read.

3.3.1 Temperature Readout

We record the temperature when the leakage current measurements are taken. A thermocouple is attached to the PC board with conductive epoxy as close as possible to the diode array. Figure 11 shows the thermocouple attached to the PC board. The kapton tape used to secure the themocouple cable is radiation hard. The thermocouple wire had to be secured to the board to prevent it from breaking the wirebonds.

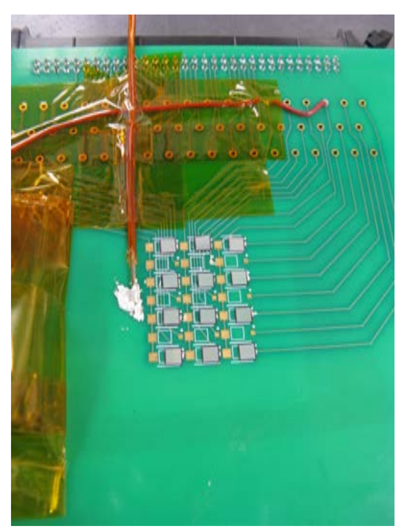

Figure 11- Thermocouple attached to diode board

3.3.2 Temperature Control

A temperature controller was built to maintain the diode board cold during the experiment at LANSCE. Compressed nitrogen is supplied through a hose to a pipe. The pipe is connected to a vortex tube. A vortex tube is a mechanical device that sends cold and hot airflow through opposite sides of the device. The cold airflow was directed to the sample box where the PC board was placed during the experiment. The box is closed everywhere except on top and in the side. The side opening is where a pressure release valve was attached. The top opening is where the vortex tube cold airflow part was mounted. Inside the sample box a pipe directed the airflow towards the center of the PC board. A temperature probe was placed close to the sensor array.

Figure 12- Temperature control setup.

Nitrogen gas was applied, and data were taken. The goal is to keep the temperature as low as possible. Figure 13 shows measurements of achievable temperature versus nitrogen flow rate. Applying 30 PSI caused the temperature to drop below 0C in less than 5 minutes. Nitrogen gas also serves to reduce humidity. Humidity can also affect the leakage current measurements.

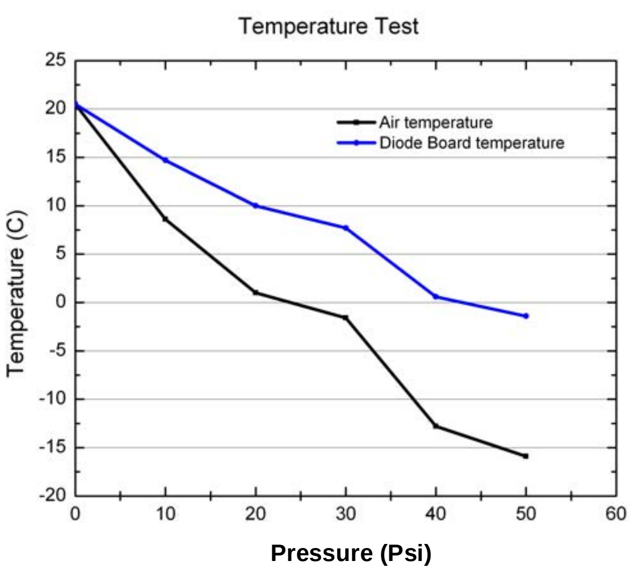

Figure 13- Temperature versus Pressure

3.2 Procedure

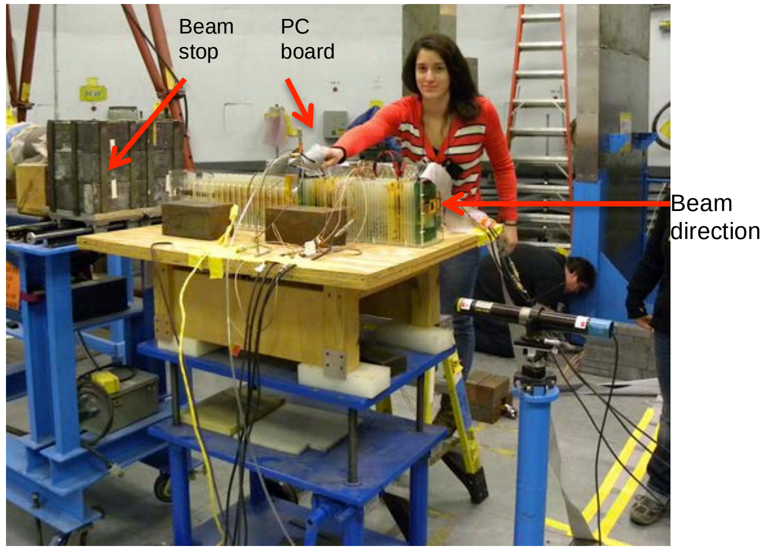

Figure14-Blue Room

The setup was brought to LANSCE, and set up inside the Blue Room (the name of the irradiation hall where the proton beam is located). Both of the Keithley devices and the switches were placed in the control room, where measurements could be made. The PC board with the 3D sensors was placed inside the Blue Room. The board was placed at the appropiate height so the 3D sensors would be transversed by the center of the beam. Figure 14 shows a picture of the Blue Room; the direction of the beam is indicated with an arrow. Two boxes with several compartments were aligned with the beam. Several samples were placed in the compartments for irradiation studies. The PC board was placed in one of the central compartments, at the end of the first box.

The control room is more than 100 feet from the Blue Room. The PC board was attached to ribbon cables running from the Blue Room to the control room which connected to the rest of the setup. After all the other samples were set up and the proton beam was calibrated, a number of runs were made. The PC board was operated for the first 12 runs. Data were recorded at the end of some of those 12 runs. The runs' duration is presented in Table 1.

Run#	duration
run1	0.5min
run2	1min
run3	2min
run4	4min
run5	1min
run6	10min
run8	19.5min
run9	52min
run11	210min
run12	240min

Table1-
Run duration

Run 1 of 30s was a test of the temperature control system. After the run the setup was inspected. Due to radiation damage the pipe connecting the vortex tube to the sample box cracked and separated from the setup. The temperature control setup was removed.

A long cable for the thermocouple was also used. The thermocouple stayed attached to the PC board during the experiments. Temperature measurements were recorded during every leakage current measurement.

In between runs measurements were performed. The appropriate bias voltage was set with the Keithley 6487. The operating voltage window had been previously estimated for certain irradiation times. After the bias voltage was set, the leakage current from each channel was read with the Keithley 6487 and recorded after every run displayed in Table 1.

The PC board was removed from the Blue Room after run 12. It was necessary to extract the sensors after run 12 because the estimated fluence the 3D sensors were going to experience during run 13 was larger than the amount they have shown they usually resist.

3.3 Analysis

After the experiment was performed, the analysis of the data was performed. The first step was to calculate the temperature scaling factor from Eq 2. For convenience T_{ref} was chosen to be 20C. The temperature of the PC board during measurements at LANSCE was 20-25C. All the measurements were scaled to 20C. The IV measurements before irradiation for all the 3D sensors were performed at 20C, so no scaling was required for these data. After ΔI was calculated, α had to be determined to complete Eq(1). Factor α is a function of temperature and time after irradiation as described in Figure 15. The time after irradiation was very short. The time dependance leads to a systematic error on α. $\alpha(\mathrm{t}=0,\mathrm{T}=20\mathrm{C})=8\pm0.03*10^{-17}\mathrm{A/cm}$[5] was the value used in the analysis.

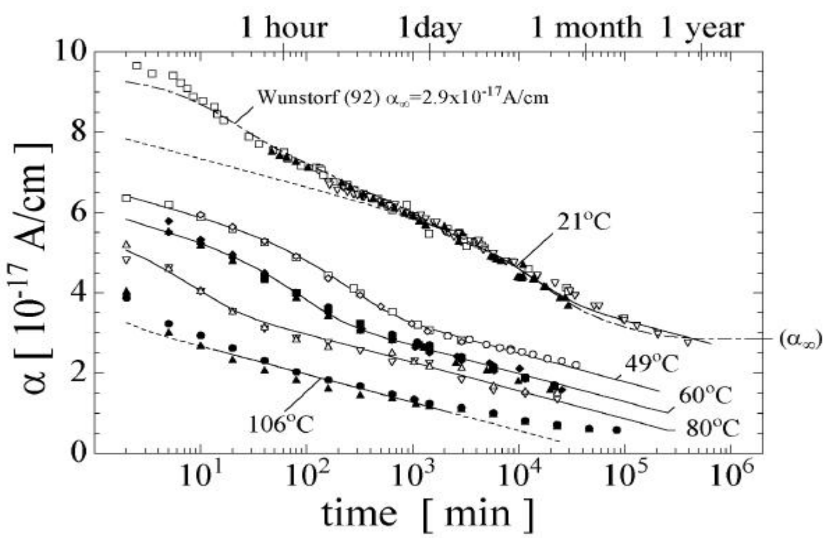

Figure15- Alpha factor temperature and time dependence (from Ref [5]).

3.4 Results

The two main objectives of this experiment were: to verify for 3D sensors the applicability of Eq 1, and to determine the conditions needed for a diode array of 3D sensors to give an accurate profile of a charged particle beam. Figure 16 shows the fluence versus beam exposure time of 2 sensors of the array: W19-5 and W19-4. The linear relationship between the fluence and beam time is apparent. The R-Square values, which are the measure of how close the data are to the fitted regression line, for W19-5 and W19-4 are 0.999 and 0.998 respectively. The fluence measured by the sensors increased linearly over 5 orders of magnitude, from $5x10^{10}$ to $5x10^{15}$ 1-MeV neutron equivalent/cm^2, with beam exposure time.

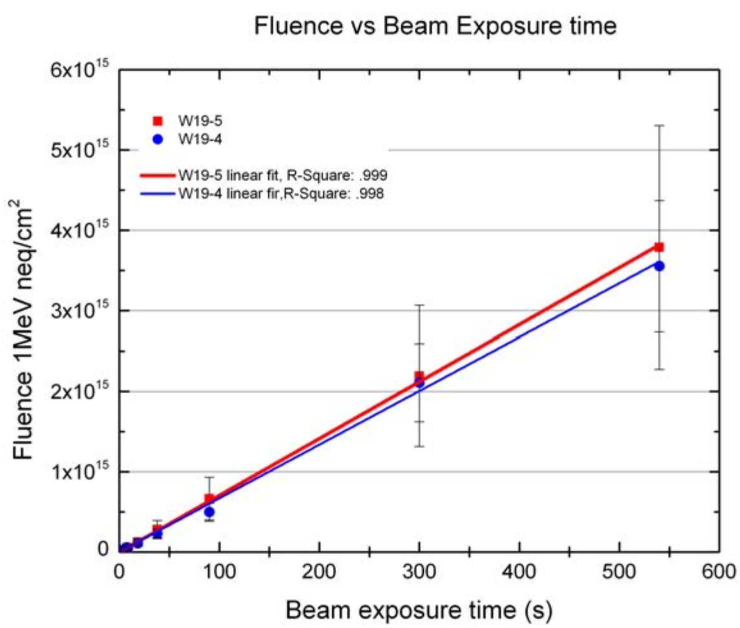

Figure 16-Fluence versus beam exposure time

Figure 17 shows the profile of the beam after 30s. The beam had a Gaussian-like shape, but it was not centered on the diode array. Sensors in the tail of the beam received fluences 7 times lower than sensors centered on the beam. Sensors in the beam spot survived fluences of more than $3.5x10^{15}$ 1-MeV-neutron equivalent/cm^2 after 540 seconds of beam exposure. Appendix 2 shows the beam profile at several other intervals.

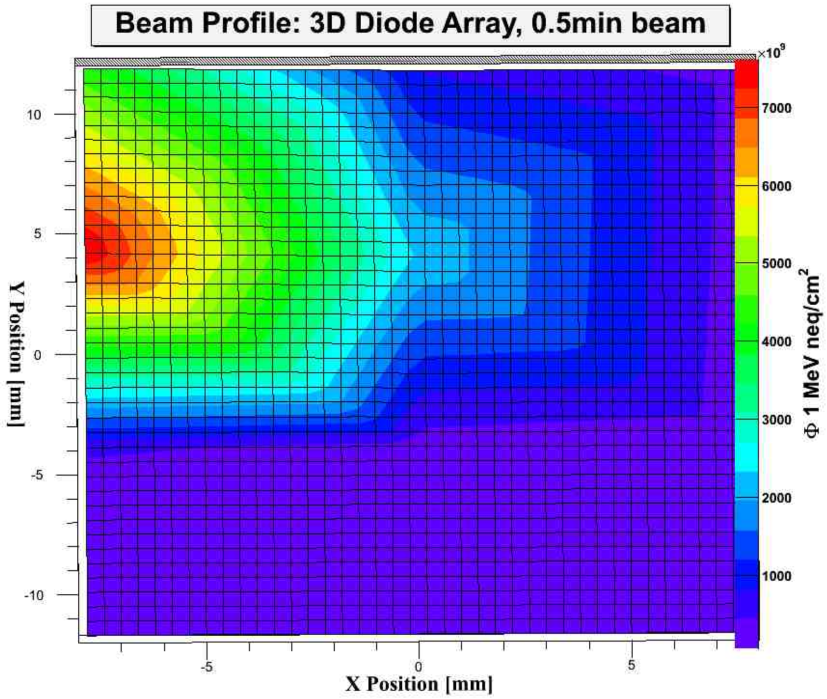

Figure 17-Profile of the beam

3.4.1 Error Analysis

Several errors contribute to the total error on the leakage current data. All the statistical errors associated with the leakage current measurements are listed in Table 2. Before each diode is mounted in the board the IV is measured 3 times. The value recorded is an average of the 3 measurements, and the error associated with that process is 0.82%. During the experiment, when the measurements were taken, the voltage was turned on while the switches were opening and closing to measure each specific channel. Three measurements were taken for each diode, and the corresponding statistical error was calculated to be 0.81%.

Statistical errors	
Type	Percentage
Sensor leakage current IV on probe station	0.82%
Irradiated sensor current versus time	0.81%

Table 2-Statistical errors on the diode array currents

All the systematic errors asociated with the leakage current measurements are listed in Table 3. Humidity affects leakage current[6]. During the experiment, humidity was not controlled. We estimate 10% to be the contribution of humidity to the current uncertainty based on a maximum relative humidity of 30%.

The error associated with the temperature is negligible. The effects of temperature were covered by multiplying by a correction factor.
Before exposing the diode array in the PC board to the proton beam, the leakage current for different voltages was recorded. The measurements were then compared to the values obtained on the probe station prior to mounting the diodes in the board. A value of 8.24% was the maximum error found due to the PC board.
Ribbon cables of more than 100 feet were used during the experiment. Several measurements were performed before irradiation with these cables. The amount of error these cables introduce was found to be 11.7%.The next 2 errors in Table 2 reflect the precision of the Keithley 6487 and Keithley 706. The devices introduce error contributions of 0.2% and 0.33% respectively. The largest source of systematic error is due to the choice of α. Parameter α depends upon the time between irradiation and measurements. We estimate an uncertainty of 15% on α.
The systematic and statistical errors were added separately in quadrature. The total systematic error was calculated to be 23.02%. The total statistical error is 1.15%. The total error on the diode array currents is 23.06%

Systematic errors	
Type	Percentage
Humidity effect on current	10%
Sensor current on PC board (short cable)	8.24%
Sensor current with long cable	11.70%
Sensor current with Keithley 6487	0.20%
Sensor current with Keithley 706	0.33%
α factor	15%

Table 3-Systematic errors on the diode array currents

3.4.2 Calibration

From the initial set of 3D diodes received for the experiment, 12 were used in the array. The rest of the working sensors were irradiated during the experiment. Each sensor was set in a bin independent from the others and correlated with an aluminum dosimetry foil. During several of the beam stops a sensor and its foil were removed. These sensors have information about the leakage current changes after irradiation. It will be possible to compare IV measurements before with IV measurements after irradiation. At the time of this writing the foils and sensors are still significantly radioactive, so they are not safe to be handled for calibration measurements. These measurements will calibrate the data since the devices had the same beam exposure times as those in Table 1.

IV. Recommendations

Bias leakage current deviations occurred due to temperature changes during the experiment. Future experiments should adjust the temperature to a colder value (0^oC) to minimize the temperature effect. Also, future experiments should perform IV and CV measurements in a cold environment. Operation at low temperature will also substantially reduce the systematic error associated with the choice of α.

Since not all the sensors in the array will receive the same fluence, their voltage operating windows can be very different. Future experiments should perform IV measurements between runs, on each sensor. The IV measurement will ensure that the device takes data in the correct voltage operating window.

V. Conclusion

The prototyped board with 3D sensors survived fluences up to the order of 10^{15} 1-MeV-neutron equivalent/cm^2 during the irradiation at Los Alamos National Lab. The radiation hard properties of the 3D were confirmed.

The 3D sensors under the beam spot were successfully operated between their depletion and breakdown voltage. Bias leakage current increased linearly with fluence as expected from Eq (1). This behavior allowed the beam profile to be obtained at different fluences.

The 3D sensors used in this study proved to be successful in measuring the beam profile and fluence from 5×10^{10} to 5×10^{15} 1-MeV-neutron equivalent/cm^2. If the recommendations are implemented it follows that the range of operation can be extended beyond 1×10^{16} 1-MeV-neutron equivalent/cm^2.

VI. References

[1] ATLAS Collaboration, JINST 3(2008) S08003.

[2] P. Palni, et al., A method for real time monitoring of charged particle beam profile and fluence, NIM-A A735 (2014) 213-217.

[3] G. Lindström, et al., Radiation hardness of silicon detectors – a challenge from high-energy physics, NIM-A A426 (1999).

[4] G.F. Dalla Betta, et al., Characterization of New FBK Double-Sided 3D Sensors with improved Breakdown Voltage, IEEE Nuclear Science Symposium, Conference Record N41-1.

[5] M.Moll, "Radiation Damage in Silicon Particle Detectors," PhD thesis, Univ. Hamburg, 1999.

[6] H. McDuff, et al., Nuclear Instruments and Methods in Physics Research A 785 (2015) 1-4.

VII. Appendix 1: CV and IV plots for all sensors

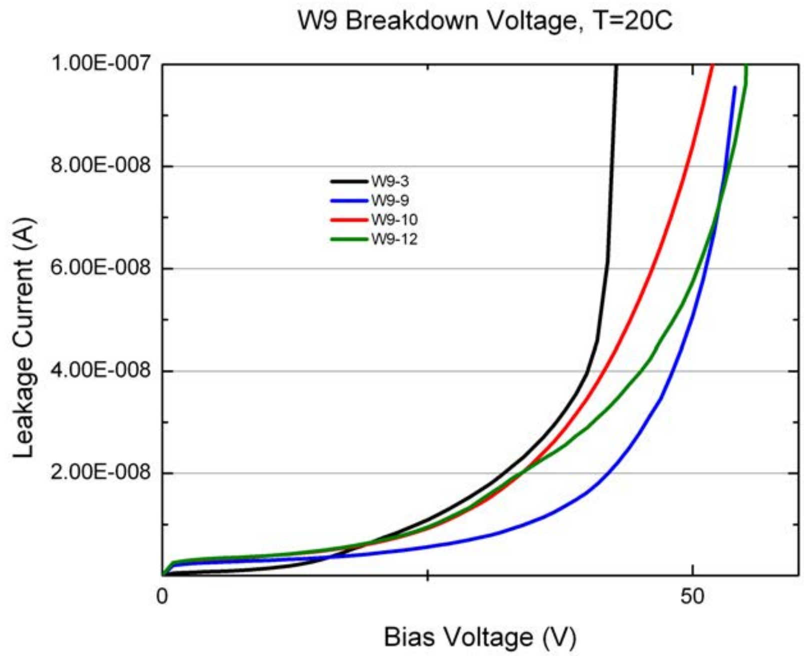

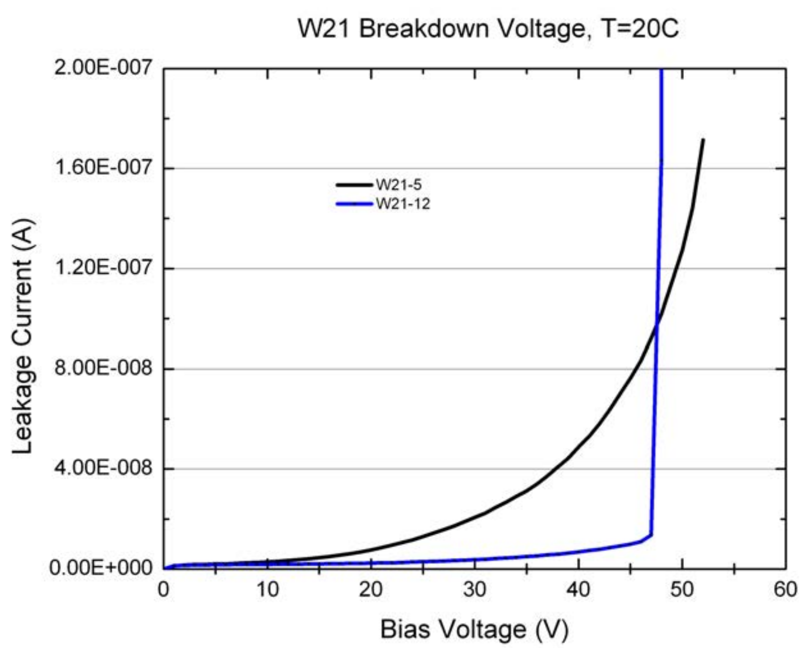

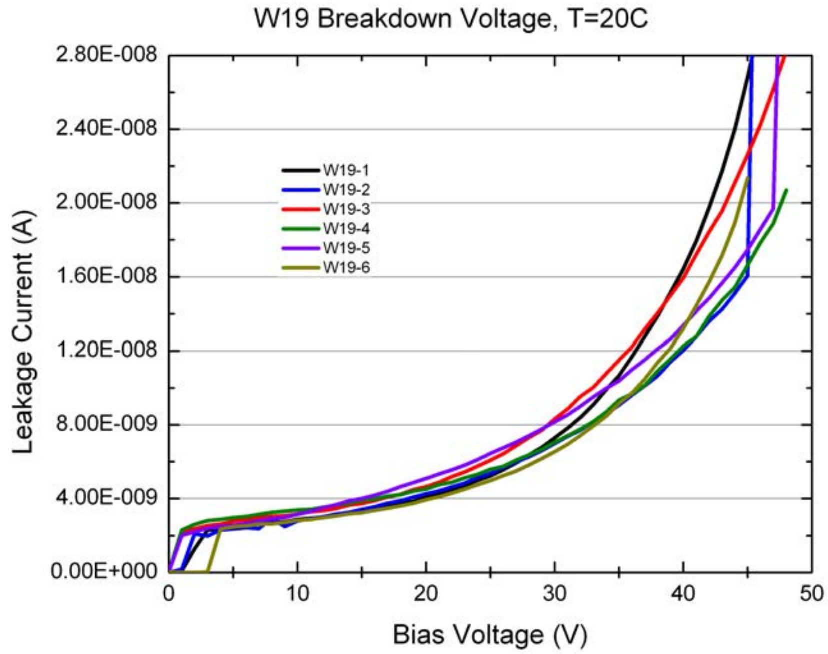
W19 Breakdown Voltage, T=20C
Leakage Current (A)
Bias Voltage (V)
W19-1
W19-2
W19-3
W19-4
W19-5
W19-6
0.00E+000
4.00E-009
8.00E-009
1.20E-008
1.60E-008
2.00E-008
2.40E-008
2.80E-008
0
10
20
30
40
50

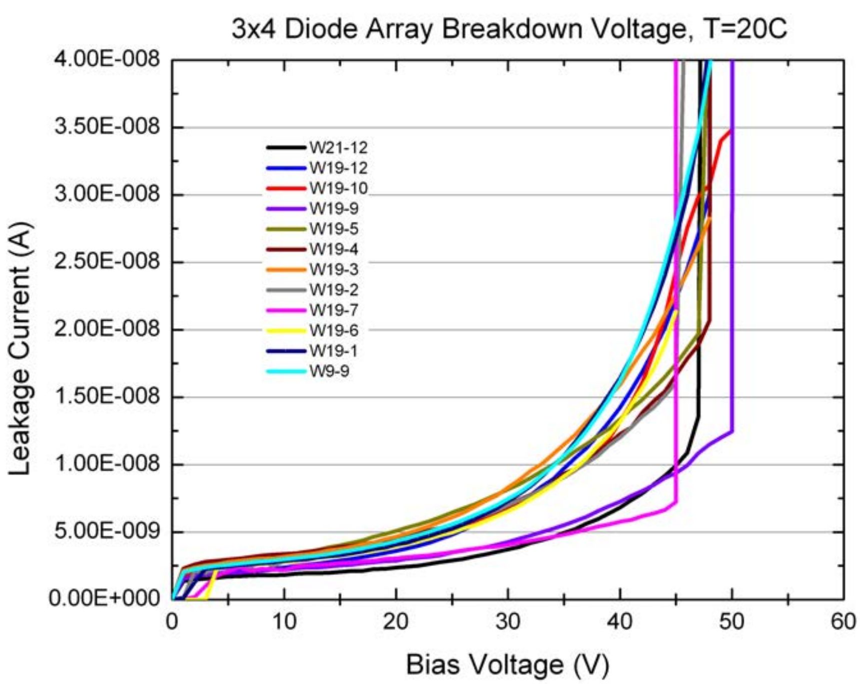
3x4 Diode Array Breakdown Voltage, T=20C
Leakage Current (A)
Bias Voltage (V)
W21-12
W19-12
W19-10
W19-9
W19-5
W19-4
W19-3
W19-2
W19-7
W19-6
W19-1
W9-9
0.00E+000
5.00E-009
1.00E-008
1.50E-008
2.00E-008
2.50E-008
3.00E-008
3.50E-008
4.00E-008
0
10
20
30
40
50
60

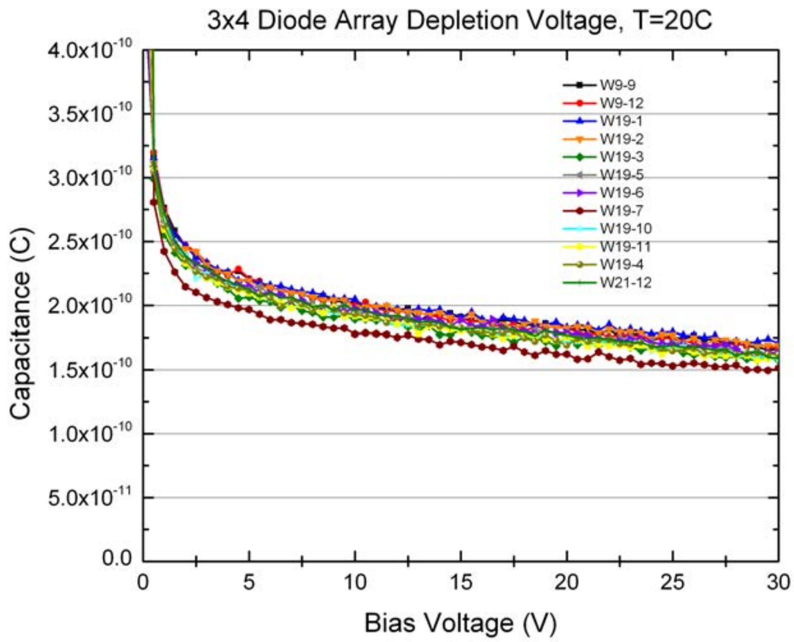
3x4 Diode Array Depletion Voltage, T=20C
W9-9
W9-12
W19-1
W19-2
W19-3
W19-5
W19-6
W19-7
W19-10
W19-11
W19-4
W21-12
Capacitance (C)
Bias Voltage (V)

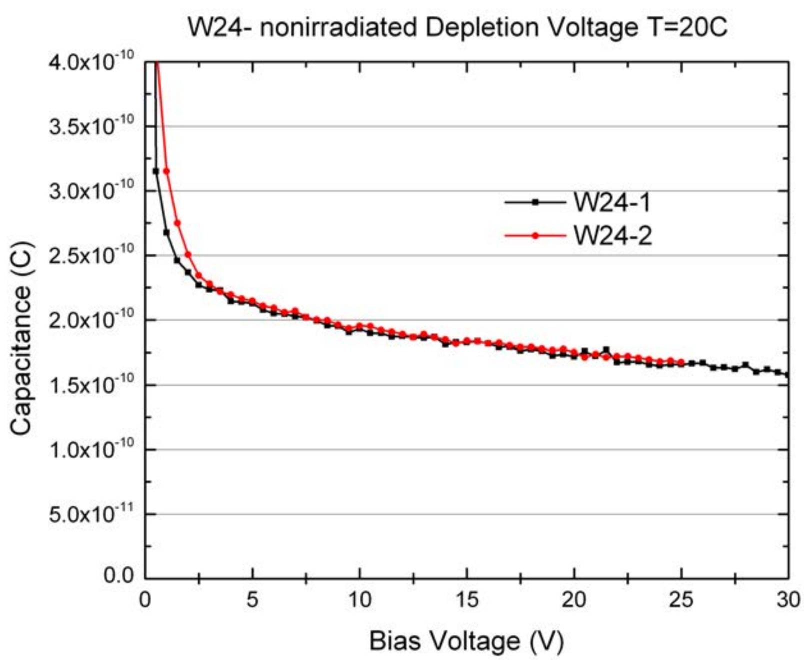
W24- nonirradiated Depletion Voltage T=20C
W24-1
W24-2
Capacitance (C)
Bias Voltage (V)

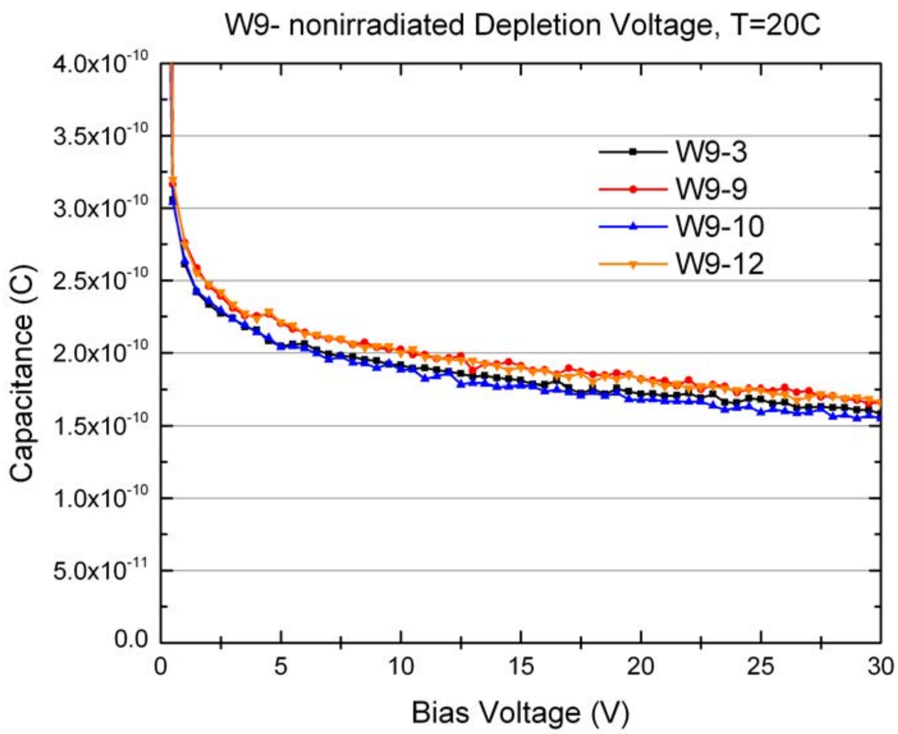
W9- nonirradiated Depletion Voltage, T=20C
Capacitance (C)
Bias Voltage (V)
W9-3
W9-9
W9-10
W9-12
4.0x10^-10
3.5x10^-10
3.0x10^-10
2.5x10^-10
2.0x10^-10
1.5x10^-10
1.0x10^-10
5.0x10^-11
0.0
0
5
10
15
20
25
30

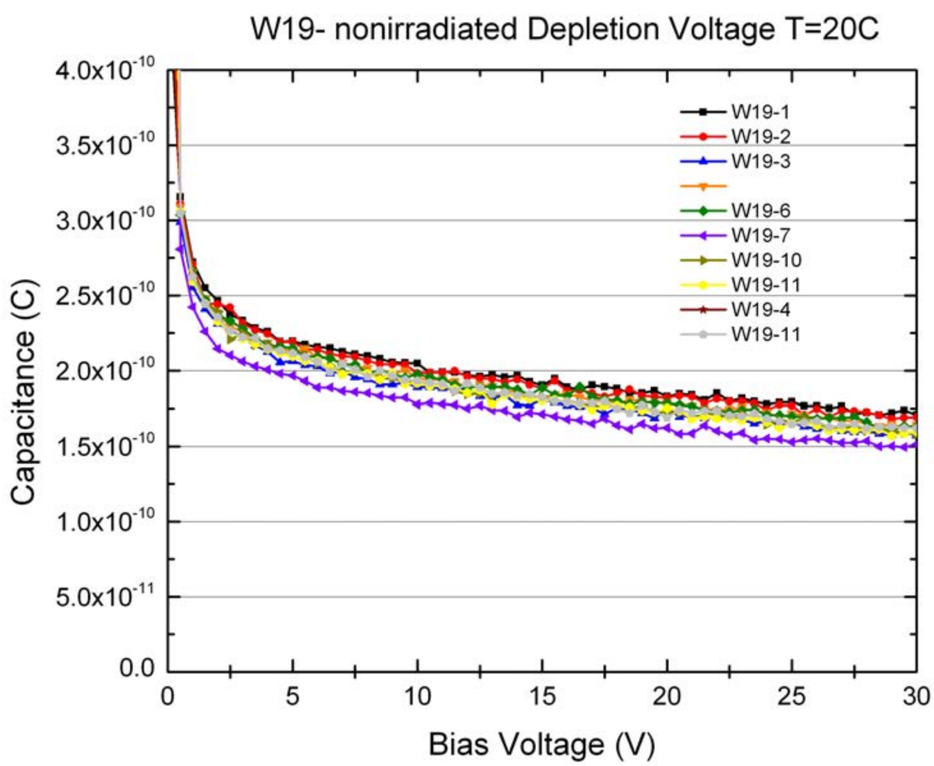
W19- nonirradiated Depletion Voltage T=20C
Capacitance (C)
Bias Voltage (V)
W19-1
W19-2
W19-3
W19-6
W19-7
W19-10
W19-11
W19-4
W19-11
4.0x10^-10
3.5x10^-10
3.0x10^-10
2.5x10^-10
2.0x10^-10
1.5x10^-10
1.0x10^-10
5.0x10^-11
0.0
0
5
10
15
20
25
30

VIII. Appendix 2: Fluence versus beam exposure time